Editors' Suggestion

Delivery of refractory radioactive ion beams via in-trap decay at ISOLDE

J. R. Reilly,[1,*] M. Athanasakis-Kaklamanakis,[2,3,†] M. Au,[1] L. Nies,[1] A. Ajayakumar,[1] M. Benhatchi,[4] J. Berbalk,[1,5] C. Bernerd,[1] K. Chrysalidis,[1] C. M. Fajardo Zambrano,[5] P. F. Giesel,[6] R. Heinke,[7] D. Lange,[8] G. Peng,[2] S. Rothe,[1] A. Schmidt,[1] C. Schweiger,[8] and J. Wessolek[1]

[1]*Systems Department, CERN, CH-1211 Geneva 23, Switzerland*
[2]*Blackett Laboratory, Centre for Cold Matter, Imperial College London, SW7 2AZ London, United Kingdom*
[3]*JILA and Department of Physics, University of Colorado, Boulder, Colorado 80309, USA*
[4]*Université Paris-Saclay, CNRS/IN2P3, IJCLab, 91405 Orsay, France*
[5]*KU Leuven, Instituut voor Kern- en Stralingsfysica, B-3001 Leuven, Belgium*
[6]*Institut für Physik, Universität Greifswald, 17489 Greifswald, Germany*
[7]*School of Physics and Astronomy, The University of Manchester, Manchester M13 9PL, United Kingdom*
[8]*Max-Planck-Institut für Kernphysik, 69117 Heidelberg, Germany*

(Received 30 April 2026; accepted 27 August 2026; published 9 November 2026)

An approach to deliver intense ion beams of refractory radioactive isotopes utilizing in-trap β^- decay is demonstrated using the gas-filled ISCOOL ion trap at CERN-ISOLDE. Ion beams of $^{97,98}Rb^+$ and $^{98}Sr^+$ were injected into the ion trap, where they underwent β^- decay and the daughter ions were successfully confined in the same trap. The produced singly charged ions were subsequently extracted and identified using the ISOLTRAP multireflection time-of-flight mass spectrometer, where the beam composition was analyzed as a function of trapping time. Modeling the observed time-dependent populations of the parent and daughter ions using the Bateman equations reproduces the isotopes' known half-lives, thereby confirming production via in-trap decay, achieving an overall efficiency for the singly charged daughter beams on the order of 1% relative to the parent intensity. Using this method, delivery of a singly charged atomic ion beam of $^{98}Y^+$ is thus reported for the first time at ISOLDE. These results demonstrate a practical and operationally simple method for delivering refractory isotopes at thick-target isotope-separation-on-line facilities, opening new opportunities for nuclear-structure studies of chemically challenging isotopes.

DOI: 10.1103/6m5s-pxyz

I. INTRODUCTION

Radioactive ion beam facilities based on the isotope separation on-line (ISOL) production method have been a cornerstone of precision experiments with radioactive nuclei for several decades [1]. Remaining at the forefront of applied and fundamental science with rare isotope beams, ISOL facilities around the world host numerous experiments on nuclear structure, nuclear astrophysics, tests of fundamental symmetries, biophysics, and materials science.

In the ISOL method, radioactive isotopes are produced by bombarding a heavy target material with energetic beams of protons or neutrons [2]. The interaction with the energetic projectiles induces fragmentation, spallation, and fission of the stable nuclei in the target, releasing thousands of radioactive isotopes across the nuclear chart as products [2]. The produced radioisotopes are contained within the matrix of the target material, so the target is heated to high temperature (1000–2200 °C depending on the material) to enable their release. The high temperature facilitates the diffusion of the radiogenic atoms through the solid material and their subsequent effusion from the surface. The radiogenic atomic vapor is then ionized using a variety of techniques [3–5], and the ions are accelerated to kinetic energies typically above 20 keV. The fast ion beam is finally mass-separated from contaminants to form a mass-purified, fast radioactive ion beam that is delivered for study.

Whether an element's radioactive isotopes can be delivered as intense ion beams at ISOL facilities strongly depends on the chemical properties of the element as a neutral atom. That is because refractory atoms do not diffuse through the target material efficiently even at high temperature, and therefore the radiogenic isotopes remain contained within the solid matrix. Reactive atoms, however, may diffuse and effuse efficiently, but tend to form a variety of molecules of different mass, leading to a large reduction in the intensity of the ion beam at any given mass-to-charge ratio. Lastly, atoms with high ionization potential can be efficiently extracted from the target

*Contact author: jordan.reilly@cern.ch
†Contact author: m.athkak@cern.ch

Published by the American Physical Society under the terms of the Creative Commons Attribution 4.0 International license. Further distribution of this work must maintain attribution to the author(s) and the published article's title, journal citation, and DOI. Open access publication funded by CERN.

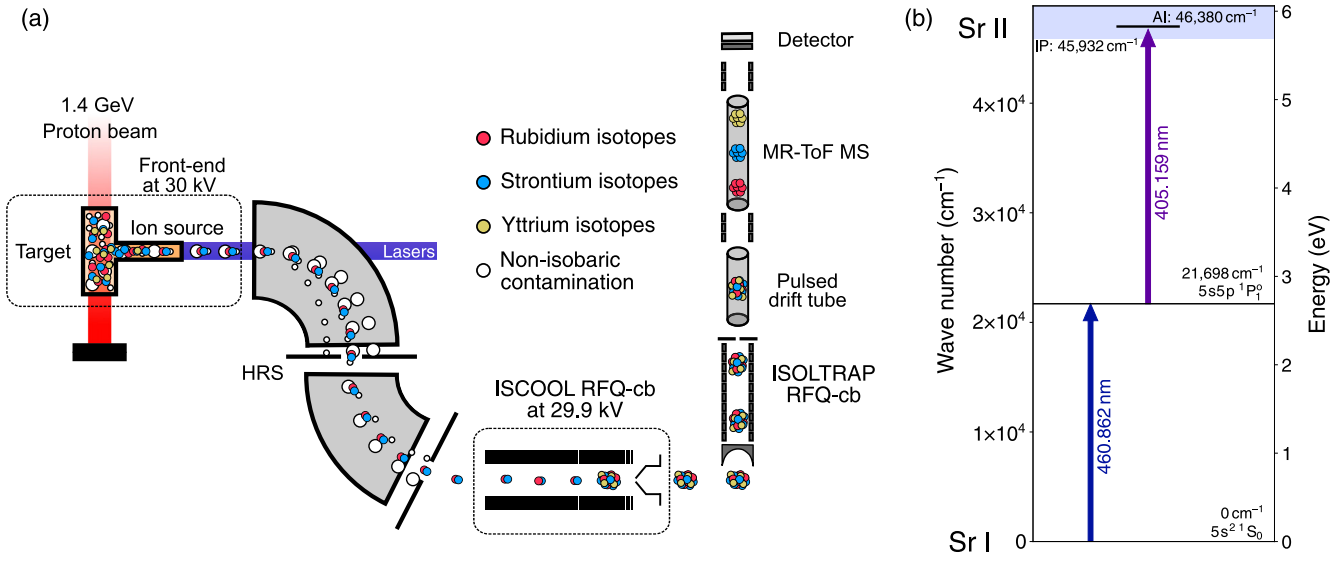


FIG. 1. Experimental setup. (a) Radioisotopes are produced in the target material by energetic collisions with 1.4-GeV proton beams. The radiogenic atoms effuse out of the target and enter the ion source, where they undergo surface or laser ionization. The ions are accelerated to ≈30 keV, purified using two magnetic dipole separators, and trapped in the gas-filled ISCOOL linear Paul trap. The trapping time within ISCOOL is varied to explore production of radioisotopes via confined in-trap decay of the injected beam. After ejection from ISCOOL, the ions are briefly rebunched in the ISOLTRAP RFQ-cb and then mass-separated in the ISOLTRAP MR-ToF MS, which provides isobaric separation with a mass-resolving power of 200 000. (b) Laser ionization scheme used to produce Sr^+ beams. For Rb^+, surface ionization is used.

without forming molecules, but require ionization via electron bombardment that typically leads to a beam full of isobaric contaminants that persist through the first stage of mass separation.

A consequence of these chemical considerations is that the short-lived isotopes of several elements cannot be delivered as ISOL-produced ion beams with sufficient intensity and chemical purity to be studied with certain experimental methods, such as various nuclear reactions techniques, solid-state investigations, and to a lesser extent, collinear laser spectroscopy. For example, several regions of the nuclear chart corresponding to refractory and reactive elements still lack extensive laser spectroscopy of their short-lived isotopes [6,7].

Here, we explore the possibility of delivering beams of refractory radioactive isotopes by first producing beams of the chemically favorable parent isotopes and confining them in a linear Paul trap with high-density helium buffer gas. The parent isotopes undergo β-decay while in the ion trap, which successfully confines the recoiling daughter isotopes and subsequently releases them as a fast ion beam. We experimentally demonstrate this approach using primary beams of $^{97,98}Rb^+$ and $^{98}Sr^+$, respectively delivering secondary beams of $^{97,98}Sr^+$ and $^{98}Y^+$ via in-trap decay.

In-trap decay has been demonstrated at ISOLDE in the past, where initial tests were performed with ^{61}Mn using the HIE-ISOLDE REXTRAP Penning trap [8] and $^{61-63}$Mn using the ISOLTRAP Penning trap [9,10]. ISOLTRAP again revisited this method to produce ^{34m}Al via in-trap decay of ^{34}Mg [11] in the Penning trap, and also by performing the decay in a linear Paul trap for decay lifetime measurements [12], but without successfully confining the decay products. Beyond ISOLDE, in-trap decay of ^{8}Li into ^{8}B in a Paul trap has been performed for weak-interaction tests [13] at Argonne National Laboratory, with a new iteration of the trap presented in Ref. [14], and at the IGISOL facility where in-trap decay was performed on ^{113}Tc [15] and ^{114}Ru [16]. In this work, we extend this approach to a general-purpose linear Paul trap at ISOLDE that can provide radioactive ion beams to all permanent and temporary experimental stations in the facility, including experiments with post-accelerated beams. We thus use this approach to produce ion beams of short-lived ^{98}Y, an isotope of the refractory element yttrium that has not been delivered as an atomic ion beam at ISOLDE so far.

II. METHODS

Figure 1(a) shows a schematic overview of the experimental setup. Radioactive isotopes across the nuclear chart are produced by impinging 1.4-GeV proton beams onto a uranium carbide target heated to 1950 °C. $^{97,98}Rb^+$ ions are produced by surface ionization of the neutral rubidium atoms via collisions with the walls of a hot tantalum capillary, heated to 2050 °C. When strontium isotopes are used as the primary beam in the ion trap, $^{98}Sr^+$ is produced by laser resonance ionization using the laser scheme shown in Fig. 1(b); no surface-ionized strontium was observed. Details on the production of radioisotopes at ISOLDE and the thermochemical processes involved can be found in Refs. [2,17].

After ionization, the radioactive isotopes are accelerated as a continuous ion beam with a kinetic energy of 30 240 eV containing isotopes of tens of elements. To remove contaminants that are not isobaric with the isotope of interest, the ion beam passes through two magnetic dipole separators that select only ions with the same mass-to-charge ratio.

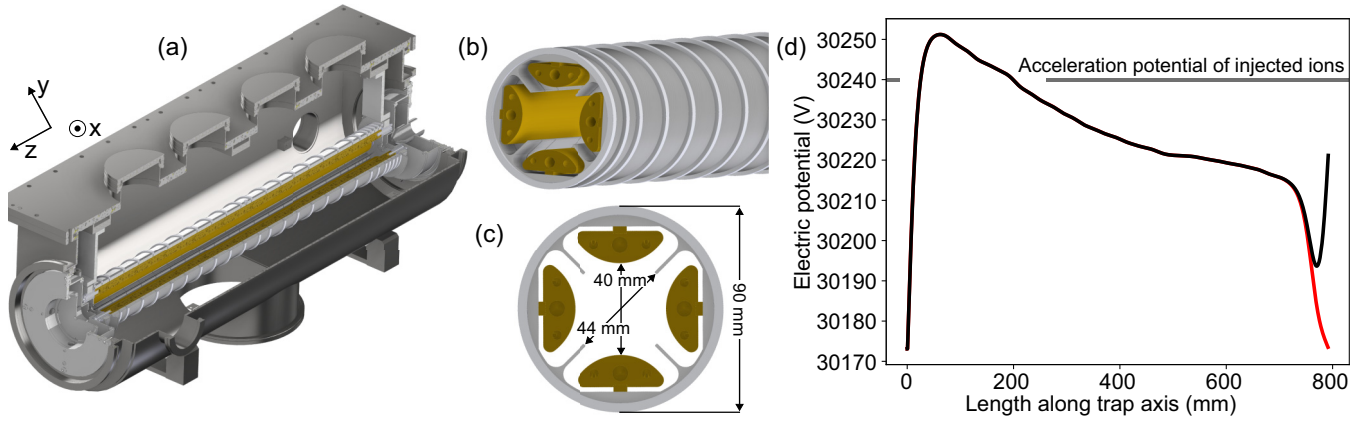


FIG. 2. ISCOOL ion trap. (a) The ion trap mounted within the vacuum chamber. (b) Oblique side view and (c) front view of the ion trap assembly. The hyperbolic electrodes (colored gold only for visual assistance) are used to create radial ($\hat{x}$-$\hat{y}$ plane) confinement by applying an RF potential, while the gray fins protruding between them are used to create the axial DC confinement along the $\hat{z}$ axis. The DC electrodes are separated by electrically insulating PEEK spacers (light gray) to create segmented axial confinement. (d) Electric potential induced by the axial electrodes along the central axis of the ion trap ($x = y = 0$), simulated using COMSOL for the electric potentials used in the experiment. The black line shows the potential profile when the final axial electrode is biased to 50 V, forming a potential well. The red line indicates the potential profile when the final axial electrode is returned to platform potential, allowing the trapped ions to be ejected.

A. ISCOOL ion trap

The mass-purified ion beam is then injected in the ISCOOL ion trap, shown in Fig. 2(a). ISCOOL is a general-purpose gas-filled linear Paul trap [18] whose key purpose is to deliver uniformly cooled ion bunches to all permanent and temporary experimental setups connected to the HRS separator at ISOLDE. Within ISCOOL, four hyperbolic electrodes [Figs. 2(b) and 2(c)] spanning the trap length are used to apply an RF potential ($\omega_{\rm rf}/2\pi = 325.62$ kHz, $V_{\rm rf} = 200$ V) that creates radial confinement of the ions. A series of twenty-five DC electrodes provide segmented axial confinement. The voltages on the axial electrodes are tuned such that the electric potential at the trap center ($x = y = 0$) along the length of the trap is as shown in Fig. 2(d).

During ion injection in ISCOOL, the first axial electrode, which is at the highest potential in the trap [see Fig. 2(d)], is set approximately 10 V higher than the acceleration potential of the injected ion beam. This set value of 10 V was obtained empirically to maximize transmission into the trap; we note that the true voltage applied to the electrode could have an offset (common for all electrodes) of a few volts with respect to the set value, and only the set voltage is referred to here. At this value, the potential of the first axial electrode provides a slowing field that decelerates the injected ions as they enter, causing them to lose kinetic energy without being reflected back. Collisions with the helium buffer gas further decrease the kinetic energy of the ions as they travel along the trap, causing them to be confined within the potential well formed when the last axial electrode is biased to 50 V [black line in Fig. 2(d)]. While in the potential well, the ions continue to collide with the helium buffer gas and are uniformly cooled to room temperature.

The voltage on the last electrode can be switched between the platform potential, shown as the red line in Fig. 2(d), and 50 V above the platform potential using a fast voltage switch, providing control over confinement or ejection of the ions. All potentials are referenced to the ISCOOL high-voltage platform at 30 240 V. The ions are ejected as a bunch, thus acquiring a pulsed structure, contrary to the continuous injected beam. As a result, ISCOOL is often referred to as a radiofrequency quadrupole cooler-buncher (RFQ-cb).

A detailed treatment of ion dynamics in linear Paul traps can be found in Refs. [19,20]. Here, only a brief summary is given for the expressions relevant to ISCOOL, which is a 2D linear Paul trap. In 2D Paul traps, radial ion confinement ($\hat{x}$-$\hat{y}$ plane) is achieved using an oscillating potential $V_{\rm rf}(x, y, t)$ of the form

$$V_{\rm rf}(x, y, t) = \frac{V_{\rm rf}^0}{R_0^2}(x^2 - y^2)\cos(\omega_{\rm rf} t), \tag{1}$$

with amplitude $V_{\rm rf}^0$, effective radial distance R_0 between the radial electrodes and the trap center, and an angular frequency $\omega_{\rm rf}$ lying in the RF range.

Axially, DC voltages are used to confine ions in an electrostatic potential well, as shown by the black solid line in Fig. 2(d), which in this case is formed toward the end of the trap after the injected ions have been sufficiently slowed. The axial DC potential has an additional antitrapping effect along $\hat{x}$ and $\hat{y}$–as a consequence of the Laplace equation $\nabla^2 V = 0$ for the total electric potential—such that the total DC potential $V_{\rm dc}(x, y, z)$ is

$$V_{\rm dc}(x, y, z) = \frac{V_{\rm dc}^0}{Z_0^2}\left(z^2 - \frac{x^2 + y^2}{2}\right), \tag{2}$$

where $V_{\rm dc}^0$ is the depth of the DC potential well and Z_0 is the effective axial distance between the axial electrodes and the minimum of the potential well.

Combining Eqs. (1) and (2) into a total electric potential and using the dimensionless transformation $\tau = \omega_{\rm rf} t/2$, the equations of motion in Cartesian coordinates can be

written as

$$\frac{\partial^2 x}{\partial \tau^2} + \left[-\frac{V_{\rm dc}^0}{2Z_0^2} + \frac{V_{\rm rf}^0}{R_0^2}\cos(2\tau) \right] \frac{8e}{m\omega_{\rm rf}^2} x = 0, \tag{3}$$

$$\frac{\partial^2 y}{\partial \tau^2} - \left[\frac{V_{\rm dc}^0}{2Z_0^2} + \frac{V_{\rm rf}^0}{R_0^2}\cos(2\tau) \right] \frac{8e}{m\omega_{\rm rf}^2} y = 0, \tag{4}$$

$$\frac{\partial^2 z}{\partial \tau^2} + \frac{V_{\rm dc}^0}{Z_0^2} \frac{8e}{m\omega_{\rm rf}^2} z = 0, \tag{5}$$

where m is the mass of a singly charged ion and e is the fundamental charge.

Equations (3)–(5), known as the Mathieu equations relevant to the 2D linear Paul trap, have the general form of

$$\frac{\partial^2 u}{\partial \tau^2} + [a_u + 2q_u \cos(2\tau)]u = 0, \tag{6}$$

where u is a Cartesian coordinate and a_u and q_u are the Mathieu parameters for coordinate u. The DC potential information is encapsulated in a_u and the RF potential information in q_u, and the two sets of parameters define the range of trap operation for which trapped-ion trajectories are bound and thus stable.

Comparing Eq. (6) with Eqs. (3)–(5), it is seen that

$$a_x = -\frac{4e}{m\omega_{\rm rf}^2}\frac{V_{\rm dc}^0}{Z_0^2}, \tag{7}$$

$$a_y = -\frac{4e}{m\omega_{\rm rf}^2}\frac{V_{\rm dc}^0}{Z_0^2}, \tag{8}$$

$$a_z = \frac{8e}{m\omega_{\rm rf}^2}\frac{V_{\rm dc}^0}{Z_0^2}, \tag{9}$$

and

$$q_x = \frac{4e}{m\omega_{\rm rf}^2}\frac{V_{\rm rf}^0}{R_0^2}, \tag{10}$$

$$q_y = -\frac{4e}{m\omega_{\rm rf}^2}\frac{V_{\rm rf}^0}{R_0^2}, \tag{11}$$

$$q_z = 0. \tag{12}$$

The ion motion in the trap can be decomposed into two parts, a slow component due to the harmonic potential that is referred to as secular motion, and a much faster, RF-driven component referred to as the RF micromotion. The Mathieu a_u and q_u parameters are related to the frequencies of secular motion of the ions in the trap, which can be calculated as

$$\Omega_u \approx \frac{\omega_{\rm rf}}{2}\sqrt{a_u + \frac{q_u^2}{2}} \tag{13}$$

for $u = x, y, z$. In turn, the secular frequencies can be related to an approximate expression for the trap depth along each coordinate axis, as

$$U_u \approx \tfrac{1}{2} m \Omega_u^2 u_{\rm max}^2, \tag{14}$$

where $u_{\rm max}$ is the maximum distance from trap center along axis $\hat{u}$ that an ion can extend to before escaping the trap.

Table I lists the values of the operational parameters of the ISCOOL linear Paul trap relevant to the present results, neglecting the impact of the buffer gas.

TABLE I. Operational parameters of the ISCOOL linear Paul trap used for in-trap decay in this work, neglecting the impact of the buffer gas.

Parameter	Value
R_0	2 cm
Z_0	2.87 cm
$V_{\rm rf}^0$	200 V
$V_{\rm dc}^0$	50 V
$\omega_{\rm rf}/2\pi$	325 kHz
$a_x = a_y$	−0.058
a_z	0.116
$q_x = -q_y$	0.48
q_z	0
$\Omega_x/2\pi = \Omega_y/2\pi$	38.9 kHz
$\Omega_z/2\pi$	55.3 kHz
$U_x = U_y$	12.1 eV
U_z	50.6 eV

B. Effect of buffer gas

The expressions presented so far assume no buffer gas within the trap volume. When adding buffer gas, the Mathieu equations are modified by the additional drag force experienced by the ions due to collisions with the neutral atoms. As a result, the effective trap depths are significantly increased in the presence of the buffer gas, leading to the successful confinement of highly energetic β-decay products within the ion trap. In Ref. [21], a modification factor for the effective trap depth of a linear Paul trap in the presence of buffer gas was introduced as

$$\tilde{U}_u = U_u \gamma^{-R_0/\lambda}, \tag{15}$$

where $\tilde{U}_u$ is the gas-modified effective trap depth and U_u is the gas-less one, and R_0 (relevant for $u = x, y$) is the effective radial distance between electrodes and trap center, as in Eq. (1). For $u = z$, R_0 should be replaced with Z_0 from Eq. (2). The parameter γ quantifies the momentum transfer between the ions of mass $m_{\rm ion}$ and buffer-gas atoms of mass $m_{\rm buffer}$, calculated as

$$\gamma = \left(\frac{m_{\rm ion} - m_{\rm buffer}}{m_{\rm ion} + m_{\rm buffer}} \right)^2, \tag{16}$$

and λ is the mean free path for ion-atom collisions from Langevin theory [21]

$$\lambda = \frac{\sqrt{2\mu}\epsilon_0 v_{\rm ion} R T_{\rm buffer}}{e\sqrt{\alpha_e} N_A P}, \tag{17}$$

where μ is the reduced mass of the ion-atom system, ϵ_0 is the permittivity of space, $v_{\rm ion}$ is the speed of the ions, R is the universal gas constant, $T_{\rm buffer}$ is the buffer-gas temperature, e is the elementary charge, α_e is the electric polarizability of the neutral atoms, N_A is Avogadro constant, and P is the buffer-gas pressure.

The ion speed $v_{\rm ion}$ of relevance to the decay-product confinement can be determined from the maximum recoil kinetic energy of the daughter nuclide in β decay, corresponding

to approximately 660, 900, and 200 eV for the decay of ^{97}Rb, ^{98}Rb, and ^{98}Sr, respectively. These recoil energy values exceed the trap depth in the absence of buffer gas, and therefore the decay product would not be confined within a gas-less trap. It is noted that recoil from internal-conversion electron emission contributes negligibly to the confinement of the decay products. Conversion electron recoil energies for the relevant decay schemes are at most a few tens of eV, substantially below the β-decay recoil energies for these ions [22].

Following Eq. (15), when helium is added to the trap at a pressure of 5×10^{-4} mbar, the trap depth in the radial direction for the trap properties of Table I is increased to approximately 1 keV for singly charged ions. This effective depth is enough to keep the decay products trapped. In ISCOOL, the 300-K helium buffer gas is injected within the enclosed trap volume using a long capillary attached to the trap at the midpoint. There is no pressure gauge directly monitoring the volume enclosed by the trap electrodes, but there is a gauge to monitor the pressure in the surrounding vacuum chamber. The ratio of the pressure in the surrounding vacuum chamber and within the enclosed trap volume has been estimated using a vacuum conductance calculation to be a factor of 239. During normal operation, the pressure in the surrounding chamber is typically around 4×10^{-6} mbar, which translates to $\approx 1 \times 10^{-3}$ mbar within the trap, which leads to successful decay product confinement.

C. Mass identification

After ejection from ISCOOL, the ion bunches are briefly rebunched in the ISOLTRAP RFQ-cb for a short duration of 10 ms for data-acquisition synchronization with the ISOLTRAP apparatus and to reduce the time spread of the bunches. The full timing sequence is shown in Fig. 3. The ISOLDE beam gate is open for 400 µs only, thereby controlling the filling window and cooling time of ISCOOL. The bunches are released with a kinetic energy of 3.2 keV before entering the multireflection time-of-flight (ToF) mass spectrometer (MR-ToF MS). The ISOLTRAP MR-ToF MS is described in detail in Ref. [23] and recent examples of its use for nuclear-structure studies with a high mass-resolving power can be found in Refs. [24–27]. The MR-ToF MS separates the isobaric contents of the ion beam into well-separated peaks in time of flight, as shown in Figs. 4(b) and 4(d). By varying the total trapping time in ISCOOL while monitoring the areas under each ToF peak with the MR-ToF MS, we investigate the delivery of ion beams of radioactive species produced and confined within the ISCOOL Paul trap from the β^- decay of the injected (parent) ions.

The MR-ToF MS was tuned to only detect singly charged ions in this work.

D. Charge state of the confined decay products

It should be noted that when a species of charge state z undergoes β^- decay, the product can be found in different charge states $z' \geqslant z$ (not to be confused with the axial coordinate z) with varying probability [28], with $z' = z + 1$ being the most probable. As a result, since the parent ions injected

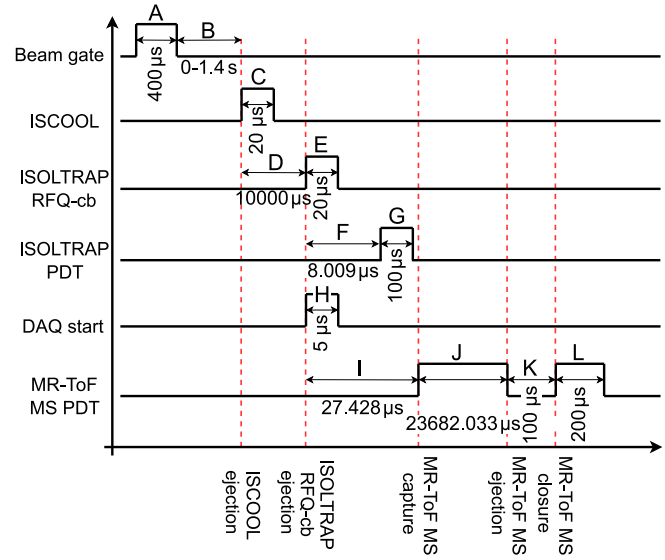


FIG. 3. Overview of the timing sequence between ISCOOL, the ISOLTRAP RFQ-cb, the ISOLTRAP pulse drift tube (PDT), and ISOLTRAP MR-ToF MS. The channel labels refer to the following: A, the ISOLDE beam gate that controls the injection window into ISCOOL, which is synchronized to the proton pulses; B, the ISCOOL cooling time; C, the ISCOOL ejection window; D, the ISOLTRAP RFQ-cb cooling time; E, the ISOLTRAP RFQ-cb ejection window; F, the ISOLTRAP PDT high-tension pulse down delay; G, the ISOLTRAP PDT high-tension pulse; H, the data acquisition start pulse; I, the MR-ToF MS cavity delay; J, the MR-ToF MS trapping time; K, the MR-ToF ejection window; and L, the MR-ToF MS reclosure window. Timings for F, I, and J are mass-dependent values and are optimized to maximize the ion signal. The ISCOOL cooling time (B) was varied from 0 to 1.4 s throughout the course of the experiment. The ISOLDE beam gate (A) duration was optimized for each A/q data set, with typical values of 10–400 µs.

in the ISCOOL ion trap have $z = +1$, the majority of the product ions are expected to be found with $z' = +2$, with a practically negligible probability of $z' = z = 1$. Indeed, the 2+ charge state directly impacts the ion confinement stability within the trap. This is highlighted in the Mathieu parameters (a_u and q_u) which scale with charge, doubling the values ($a_x = a_y = -0.116, q_x = 0.96$). This would result in the ion falling close to the edge of the stability region.

As the MR-ToF MS was tuned to detect singly charged ions, successfully detected decay products have undergone a charge exchange process within the trap. It is likely that the charge exchange process occurs via collisions with a neutral atom or molecule present in the buffer gas. The efficiency of the charge exchange process is governed by the energy defect (ΔE) between the ionization potential of the charged particle (IP_2) and the neutral particle (IP_1). Efficient charge exchange occurs when $\Delta E = IP_2 - IP_1$ is near zero. In this work, the resulting decay products confined within the trap are Sr^{2+} ($IP_2 \approx 11$ eV) and Y^{2+} ($IP_2 \approx 12.2$ eV), which have a significantly different ionization potential compared to He ($IP_1 \approx 24.6$ eV) [29]. Therefore, the large ΔE indicates inefficient charge exchange. Alternatively, trace contaminants such as O_2, H_2O, CH_4, CO, and CO_2 all possess

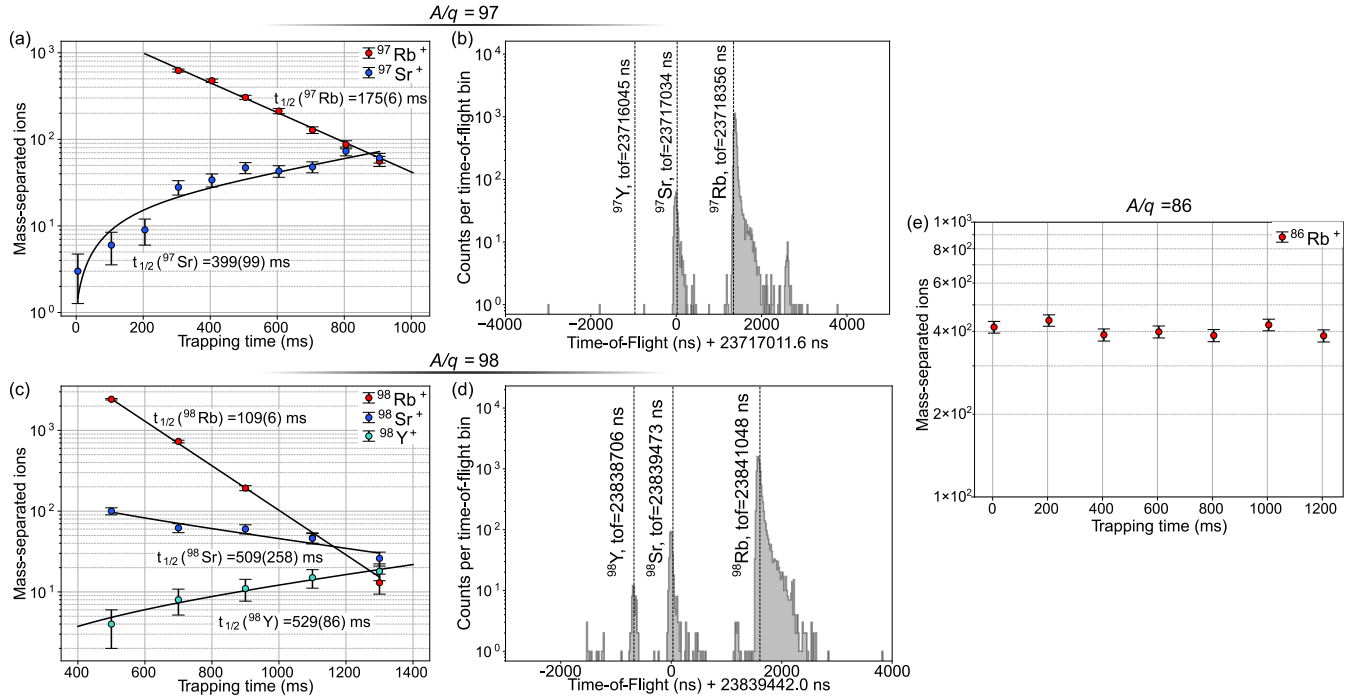


FIG. 4. Population of Rb^+, Sr^+, and Y^+ detected with the MR-ToF MS. (a) Evolution of ion counts with mass-to-charge ratio of $A/q = 97$ as a function of trapping time in ISCOOL. The y-axis corresponds to the total ions recorded across all shots for each trapping time. (b) Mass-separated MR-ToF peaks for ions with $A/q = 97$, integrated across all trapping times in panel (a). Panels (c) and (d) are similar to panels (a) and (b), respectively, for ions with mass-to-charge ratio of $A/q = 98$. (e) Population of $^{86g+}$Rb (half-life $t_{1/2} = 18.7$ days) ions separated with the MR-ToF MS as a function of trapping time in ISCOOL.

$IP_1 \approx 12.1$–14.0 eV [30]. In particular, O_2 possesses a near-resonant $IP_1 = 12.07$ eV with Y^{2+}, where the energy defect is $\Delta E = +0.13$ eV. Consequently, it is suggested that the charge exchange process is more likely to occur with the trace contaminants than with the He buffer gas itself, since it gives a more energetically plausible mechanism for the observed charge-state reset.

III. RESULTS

In the measurements presented here, the decay chains of interest are $^{97}Rb \rightarrow {}^{97}Sr$ [$t_{1/2} = 169.1(6)$ ms $\rightarrow 431(5)$ ms] and $^{98}Rb \rightarrow {}^{98}Sr \rightarrow {}^{98}Y$ [$t_{1/2} = 115(6)$ ms $\rightarrow 653(2)$ ms $\rightarrow 548(1)$ ms], where the half-lives are taken from NuDat 3 [31]. Figure 4 shows that $^{97,98}Sr^+$ and $^{98}Y^+$ ion beams produced via the confined β^- decay of their parent isotopes (^{97,98}Rb and ^{98}Sr, respectively) within ISCOOL were successfully delivered to ISOLTRAP. In Figs. 4(a) amd 4(b), the laser ionization scheme for Sr [Fig. 1(b)] was not applied, and as a result the ion beam does not contain $^{97}Sr^+$ for short ISCOOL trapping times. As the ions are being trapped for longer durations within ISCOOL, the population of $^{97}Rb^+$ delivered to the ISOLTRAP MR-ToF MS decays exponentially, while the population of $^{97}Sr^+$ increases. It is noted that the $^{97}Rb^+$ ion counts in Fig. 4(a) are truncated such that data points corresponding to very short trapping times are ignored due to the high ion number, which leads to detector saturation.

The population of $^{97}Rb^+$ is not being fed by the decay of another isotope in the ion trap. Therefore, $^{97}Rb^+$ acts as a parent nuclide and its ion counts can be fitted with a simple exponential function of the form:

$$N_1(t) = N_1(0)e^{-\lambda t} + C, \tag{18}$$

where $N_1(0)$ is the initial population of the nuclide, λ is the decay constant that is related to the nuclide's half-life as $t_{1/2} = \ln 2/\lambda$, and C is a constant background term.

The population of $^{97}Sr^+$, however, is being fed by the decay of $^{97}Rb^+$ in the ISCOOL ion trap, while also undergoing radioactive decay of its own. As a result, its description over time requires the use of the solution to the two-species Bateman equations:

$$N_2(t) = \epsilon_{12}N_1(0)\frac{\lambda_1}{\lambda_2 - \lambda_1}(e^{-\lambda_1 t} - e^{-\lambda_2 t}) + N_2(0)e^{-\lambda_2 t} + C, \tag{19}$$

with isotope 1 being the parent nuclide and isotope 2 the daughter. ϵ_{12} is the efficiency of confining the daughter nuclide in the trap, and $\epsilon_{12}N_1(0)$ can be treated as a single amplitude.

Equation (18) is fitted to the $^{97}Rb^+$ data and Eq. (19) to the $^{97}Sr^+$ data in Fig. 4(a). Since no $^{97}Y^+$ ions were detected, a three-species Bateman equation for the granddaughter isotope is not needed. The absence of $^{97}Y^+$ is consistent with the findings presented in this work. Firstly, since no laser ionization scheme was employed for Sr during the $A/q = 97$ measurement, $^{97}Sr^+$ is seen only due to the in-trap β-decay of $^{97}Rb^+$. Therefore, any production of $^{97}Y^+$ would arise from

a second sequential decay (^{97}Rb → ^{97}Sr → ^{97}Y). A two-step decay chain would compound the confinement inefficiencies of each individual decay step and is therefore expected to yield a substantially smaller population than the single-decay case. Furthermore, there is a 15% branching ratio for the decay of ^{97}Sr to the $(9/2)^+$ isomeric state in ^{97}Y ($t_{1/2} = 1.17$ s), which predominantly decays to ^{97}Zr rather than by γ emission to the ^{97}Y ground state [32]. Trapping times on the order of 900 ms would result in a large fraction of ^{97m}Y decaying to ^{97}Zr while being confined within ISCOOL. These combined factors can account for the absence of ^{97}Y$^+$ under the present experimental conditions.

In the case of the mass-to-charge ratio $A/q = 98$ data [Figs. 4(c) and 4(d)], the in-source laser ionization scheme for Sr was used, leading to an initial population of ^{98}Sr$^+$ in the ion trap. In this case, ^{98}Y$^+$ ions were detected in the MR-ToF MS, resulting in the three nuclide populations as a function of ISCOOL trapping time, as shown in Fig. 4(c). The populations of ^{98}Rb$^+$ and ^{98}Sr$^+$ can be described using Eqs. (18) and (19), respectively, as with the $A/q = 97$ data. The population of ^{98}Y$^+$ can be analyzed with the three-species analog of Eq. (19) that describes the population evolution of the granddaughter nuclide. In the analysis of ^{98}Y$^+$ in Fig. 4(c) we find that the half-life of ^{98}Y agrees with the NuDat 3 value only if the initial population of ^{98}Rb$^+$ in the three-species Bateman equation is consistent with zero (either by explicit constraint or by chi-squared minimization). In that case, the time evolution of ^{98}Y$^+$ is simply described by Eq. (19). This implies that the detected ^{98}Y$^+$ ions do not originate from two successive β^- decays starting from ^{98}Rb$^+$. Instead, ^{98}Y$^+$ ions are produced via a single in-trap β^- decay of the ^{98}Sr$^+$ ions that are initially present in the ion trap, produced with laser ionization in the ion source. This is consistent with the fact that no ^{97}Y$^+$ is seen in the $A/q = 97$ data, where the laser ionization scheme of Sr was not used.

Figure 4(e) shows the evolution of ^{86}Rb$^+$ ions measured with the MR-ToF MS as a function of trapping time in ISCOOL. ^{86}Rb has a half-life of 18.7 days, and therefore no detectable change in the ion counts is expected due to radioactive decay for the studied trapping timescale. Indeed, no statistically significant loss is observed for ^{86}Rb$^+$, which indicates that radioactive decay is the dominant mechanism for the parent-ion loss in Figs. 4(a) and 4(c) since other loss mechanisms are negligible. It is noted that ISCOOL parameters are optimized for each mass-to-charge ratio in Fig. 4.

In Table II, the half-lives of the isotopes extracted from the data in Fig. 4 are compared to the values listed in the NuDat 3 database [31]. Agreement within 1σ is found in all cases.

As seen in Fig. 4, for sufficiently long trapping times within ISCOOL, the singly charged ion beam of the daughter isotope can reach an intensity on the order of $1 - 2\%$ compared to the initial population of the parent isotope at very short trapping times. We therefore consider an efficiency on the order of a percent for the in-trap-decay production of daughter isotopes with the same atomic charge state as the parent. We note that the absolute ion counts in Fig. 4 do not represent the full intensity of the ion beams. The intensity of the ion beams injected into the MR-ToF MS was reduced using an electrostatic beam gate to prevent peak coalescence in mass separation and damaging the ion detector. Considering that the full intensity of the parent beams of ^{97,98}Rb$^+$ and ^{98}Sr$^+$ was measured using a Faraday cup to be approximately 1×10^7 ions per second for each isotope, the source-equivalent intensity of the ^{98}Y$^+$ ion beam produced via in-trap decay was on the order of 1×10^5 ions per second. Under realistic settings, only a fraction of the daughter beam can be delivered for future study at the different experimental setups at ISOLDE, since delivering the full intensity would require trapping the parent ion beam in ISCOOL at its maximum intensity, which can be challenging due to space-charge effects. However, the delivered intensity is still sufficient for the application of several experimental techniques used in nuclear physics.

TABLE II. Comparison between isotope half-lives measured via in-trap decay in this work and the values listed in the NuDat 3 database.

	Half-life $t_{1/2}$ (ms)	
	In-trap decay analysis	NuDat 3 [31]
^{97}Rb	175(6)	169.1(6)
^{97}Sr	399(99)	431(5)
^{98}Rb	109(6)	115(6)
^{98}Sr	509(258)	653(2)
^{98g}Y	529(86)	548(1)

Since the MR-ToF MS is set to detect only singly charged ions for the mass-to-charge ratios we are interested in, successful detection of in-trap decay in this work relies on a single charge-exchange reaction taking place between neutral atoms present in the buffer gas and the decay products, which are primarily emitted as doubly charged ions. The ion charge-state distribution can also be affected by internal conversion, where the resulting atomic-shell electron vacancy may relax via Auger emission [33], consequently producing charge states higher than $z + 1$ and thus requiring further neutralization. A full investigation of this effect is beyond the scope of the present work.

For the decay products to be successfully detected by the MR-ToF MS, they must undergo a charge-exchange reaction with contaminants present in the high-purity He buffer gas. At the same time, we do not observe any losses of the primary singly charged ions due to neutralizing reactions [see Fig. 4(e)], indicating a very small cross section for singly charged ions moving at speeds defined by their secular motion within the trap. Due to the high kinetic energy of the decay products immediately after β decay, the reaction rate can be enhanced by several orders of magnitude. Therefore, it is possible that the fast doubly charged decay products react with the neutral atoms at an enhanced rate, while the singly charged ions do not undergo a reaction within the trapping timescale of relevance to these results. However, we note that a rigorous quantitative investigation is needed to confirm this.

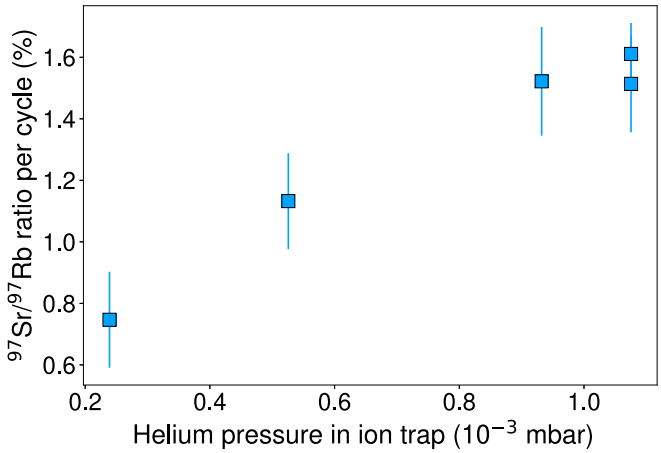


FIG. 5. Ratio of $^{97}Sr^{+}$ ions produced via in-trap decay to the $^{97}Rb^{+}$ parent ions within ISCOOL, as a function of the expected buffer-gas pressure within the trap volume. The ions were trapped in ISCOOL for 785 ms and the counts are measured following mass separation using the ISOLTRAP MR-ToF MS.

Slowing down and confining the fast β^{-} decay products within ISCOOL strongly depends on the buffer-gas pressure within the trap volume. Collisions with the buffer gas provide a drag force that can quickly reduce the kinetic energy of the decay products. Therefore, it can be expected that increasing the buffer-gas pressure in the trap has a strong effect on the product confinement efficiency, until a saturation level is reached. The rate of charge-exchanging collisions between the ions and the buffer gas is also dependent on the gas pressure. Based on numerical estimates using Eq. (15), a helium pressure of 5×10^{-4} mbar within the trap volume is enough to increase the effective trap depth to approximately 1 keV, which suffices for trapping the decay products considered here. Figure 5 shows how the ratio of $^{97}Sr^{+}$ ions produced via in-trap decay of $^{97}Rb^{+}$ changes as a function of the buffer-gas pressure within the trap volume, after being trapped for 785 ms. Due to technical reasons, a limited set of pressure values could be used and included in Fig. 5. It is seen that a fivefold increase in the gas pressure induces only a twofold increase in the decay-product ratio.

Additionally, the pressure of diminishing returns roughly agrees with the estimate for the pressure threshold from Eq. (15).

While Fig. 5 does not disentangle the product-confinement efficiency from the charge-exchange reaction efficiency, the results indicate that a further increase in buffer-gas pressure will not lead to improved confinement efficiency for the decay products. On the contrary, further increasing the buffer-gas pressure would likely result in a reduction in the overall capture and trapping efficiency of the parent ions.

IV. CONCLUSION

Singly charged $^{97,98}Sr^{+}$ and $^{98}Y^{+}$ beams were produced through the in-trap decay of $^{97,98}Rb^{+}$ and $^{98}Sr^{+}$, respectively. This constitutes the first delivery of an atomic $^{98}Y^{+}$ beam at ISOLDE. While molecular extraction is compatible with decay spectroscopy, mass spectrometry, and often nuclear reaction experiments, laser spectroscopy is species-sensitive and atomic ion beams are often preferred over molecular ones. Therefore, in-trap decay offers a complementary production method for specialized cases, including atomic ion beams of refractory species. An efficiency at the percent level is demonstrated for the delivery of singly charged atomic ion beams produced via in-trap decay of singly charged parent beams. The main limitation of this approach will remain with the maximum beam intensity that can be injected into ISCOOL due to space charge effects, even if the efficiencies are improved in the future.

Crucially, this approach requires no modification to the existing target or ion source and utilizes the existing beamline infrastructure at ISOLDE, making it immediately applicable to other favorable parent-daughter decay chains. Based on the chemical accessibility of the parent isotopes and their decay properties, other promising candidates for future in-trap decay studies are Mn → Fe, Ga → Ge, Ba → La, and Lu → Hf, for several of which the daughters remain largely inaccessible by precision laser spectroscopy techniques due to their refractory nature.

ACKNOWLEDGMENTS

We thank the ISOLTRAP collaboration and the technical teams at ISOLDE for their support. This project has received funding from the European Union's Horizon Europe Research and Innovation programme under Grant Agreement No. 101057511 (EURO-LABS).

DATA AVAILABILITY

The data that support the findings of this article are not publicly available. The data are available from the authors upon reasonable request.

[1] Y. Blumenfeld, T. Nilsson, and P. Van Duppen, Facilities and methods for radioactive ion beam production, Phys. Scr. **T152**, 014023 (2013).

[2] U. Köster, Intense radioactive-ion beams produced with the ISOL method, Eur. Phys. J. A **15**, 255 (2002).

[3] R. Kirchner, Review of ISOL target–ion-source systems, Nucl. Instrum. Methods Phys. Res., Sect. B **204**, 179 (2003).

[4] U. Köster, O. Arndt, E. Bouquerel, V. Fedoseyev, H. Frånberg, A. Joinet, C. Jost, I. Kerkines, and R. Kirchner, Progress in ISOL target-ion source systems, Nucl. Instrum. Methods Phys. Res., Sect. B **266**, 4229 (2008).

[5] V. Fedosseev, K. Chrysalidis, T. D. Goodacre, B. Marsh, S. Rothe, C. Seiffert, and K. Wendt, Ion beam production and study of radioactive isotopes with the laser ion source at ISOLDE, J. Phys. G: Nucl. Part. Phys. **44**, 084006 (2017).

[6] P. Campbell, I. Moore, and M. Pearson, Laser spectroscopy for nuclear structure physics, Prog. Part. Nucl. Phys. **86**, 127 (2016).

[7] X. Yang, S. Wang, S. Wilkins, and R. G. Ruiz, Laser spectroscopy for the study of exotic nuclei, Prog. Part. Nucl. Phys. **129**, 104005 (2023).

[8] J. Van de Walle, V. Bildstein, N. Bree, J. Cederkäll, P. Delahaye, J. Diriken, A. Ekström, V. Fedosseev, R. Gernhäuser, A. Gustafsson, A. Herlert, M. Huyse, O. Ivanov, T. Kröll, R. Krücken, B. Marsh, N. Partronis, P. Van Duppen, D. Voulot, and S. Lenzi, In-trap decay of ^{61}Mn and Coulomb excitation of ^{61}Mn / ^{61}Fe, Eur. Phys. J. A **42**, 401 (2009).

[9] A. Herlert, D. Beck, K. Blaum, F. Carrel, P. Delahaye, S. George, C. Guénaut, F. Herfurth, A. Kellerbauer, H.-J. Kluge, D. Lunney, M. Mukherjee, L. Schweikhard, and C. Yazidjian, Mass spectrometry of atomic ions produced by in-trap decay of short-lived nuclides, New J. Phys. **7**, 44 (2005).

[10] A. Herlert, S. Gorp, D. Beck, K. Blaum, M. Breitenfeldt, R. Cakirli, S. George, U. Hager, F. Herfurth, A. Kellerbauer, D. Lunney, R. Savreux, L. Schweikhard, and C. Yazidjian, Recoil-ion trapping for precision mass measurements, Eur. Phys. J. A **48**, 97 (2012).

[11] P. Ascher, N. Althubiti, D. Atanasov, K. Blaum, R. B. Cakirli, S. Grévy, F. Herfurth, S. Kreim, D. Lunney, V. Manea, D. Neidherr, M. Rosenbusch, L. Schweikhard, A. Welker, F. Wienholtz, R. N. Wolf, and K. Zuber, Mass measurements of neutron-rich isotopes near $N = 20$ by in-trap decay with the ISOLTRAP spectrometer, Phys. Rev. C **100**, 014304 (2019).

[12] R. Wolf, D. Atanasov, K. Blaum, S. Kreim, D. Lunney, V. Manea, M. Rosenbusch, L. Schweikhard, A. Welker, F. Wienholtz, and K. Zuber, Background-free beta-decay half-life measurements by in-trap decay and high-resolution MR-ToF mass analysis, Nucl. Instrum. Methods Phys. Res., Sect. B **376**, 275 (2016).

[13] M. T. Burkey, G. Savard, A. T. Gallant, N. D. Scielzo, J. A. Clark, T. Y. Hirsh, L. Varriano, G. H. Sargsyan, K. D. Launey, M. Brodeur, D. P. Burdette, E. Heckmaier, K. Joerres, J. W. Klimes, K. Kolos, A. Laminack, K. G. Leach, A. F. Levand, B. Longfellow, B. Maaß, *et al.*, Improved limit on tensor currents in the weak interaction from ^{8}Li β decay, Phys. Rev. Lett. **128**, 202502 (2022).

[14] L. Varriano, G. Savard, J. Clark, D. Burdette, M. Burkey, A. Gallant, T. Hirsh, B. Longfellow, N. Scielzo, R. Segel, E. Boron, M. Brodeur, N. Callahan, A. Cannon, K. Kolos, B. Liu, S. Lopez-Caceres, M. Gott, B. Maaß, S. Marley, *et al.*, The beta-decay Paul trap Mk IV: Design and commissioning, Nucl. Instrum. Methods Phys. Res., Sect. A **1058**, 168818 (2024).

[15] M. Hukkanen, W. Ryssens, P. Ascher, M. Bender, T. Eronen, S. Grévy, A. Kankainen, M. Stryjczyk, L. Al Ayoubi, S. Ayet, O. Beliuskina, C. Delafosse, Z. Ge, M. Gerbaux, W. Gins, A. Husson, A. Jaries, S. Kujanpää, M. Mougeot, D. A. Nesterenko, *et al.*, Binding energies of ground and isomeric states in neutron-rich ruthenium isotopes: Measurements at JYFLTRAP and comparison to theory, Phys. Rev. C **108**, 064315 (2023).

[16] M. Stryjczyk, A. Jaries, W. Ryssens, M. Bender, A. Kankainen, T. Eronen, Z. Ge, I. Moore, M. Mougeot, A. Raggio, and J. Ruotsalainen, Discovery of a new long-lived isomer in ^{114}Rh via Penning-trap mass spectrometry, Phys. Lett. B **862**, 139359 (2025).

[17] U. Köster, ISOLDE target and ion source chemistry, Radiochimica Acta **89**, 749 (2001).

[18] E. Mané, J. Billowes, K. Blaum, P. Campbell, B. Cheal, P. Delahaye, K. T. Flanagan, D. H. Forest, H. Franberg, C. Geppert, T. Giles, A. Jokinen, M. Kowalska, R. Neugart, G. Neyens, W. Nörtershäuser, I. Podadera, G. Tungate, P. Vingerhoets, and D. T. Yordanov, An ion cooler-buncher for high-sensitivity collinear laser spectroscopy at ISOLDE, Eur. Phys. J. A **42**, 503 (2009).

[19] W. Paul, Electromagnetic traps for charged and neutral particles, Rev. Mod. Phys. **62**, 531 (1990).

[20] D. Leibfried, R. Blatt, C. Monroe, and D. Wineland, Quantum dynamics of single trapped ions, Rev. Mod. Phys. **75**, 281 (2003).

[21] W. Xu, Q. Song, S. A. Smith, W. J. Chappell, and Z. Ouyang, Ion trap mass analysis at high pressure: A theoretical view, J. Am. Soc. Mass Spectrom. **20**, 2144 (2009).

[22] T. Kibédi, T. W. Burrows, M. B. Trzhaskovskaya, P. M. Davidson, and C. W. Nestor, Evaluation of theoretical conversion coefficients using BrIcc, Nucl. Instrum. Methods Phys. Res., Sect. A **589**, 202 (2008).

[23] R. Wolf, F. Wienholtz, D. Atanasov, D. Beck, K. Blaum, C. Borgmann, F. Herfurth, M. Kowalska, S. Kreim, Y. A. Litvinov, D. Lunney, V. Manea, D. Neidherr, M. Rosenbusch, L. Schweikhard, J. Stanja, and K. Zuber, ISOLTRAP's multi-reflection time-of-flight mass separator/spectrometer, Int. J. Mass Spectrom. **349-350**, 123 (2013).

[24] L. Nies, D. Atanasov, M. Athanasakis-Kaklamanakis, M. Au, K. Blaum, J. Dobaczewski, B. S. Hu, J. D. Holt, J. Karthein, I. Kulikov, Y. A. Litvinov, D. Lunney, V. Manea, T. Miyagi, M. Mougeot, L. Schweikhard, A. Schwenk, K. Sieja, and F. Wienholtz, Isomeric excitation energy for ^{99}In^{m} from mass spectrometry reveals constant trend next to doubly magic ^{100}Sn, Phys. Rev. Lett. **131**, 022502 (2023).

[25] L. Nies, L. Canete, D. D. Dao, S. Giraud, A. Kankainen, D. Lunney, F. Nowacki, B. Bastin, M. Stryjczyk, P. Ascher, K. Blaum, R. B. Cakirli, T. Eronen, P. Fischer, M. Flayol, V. Girard Alcindor, A. Herlert, A. Jokinen, A. Khanam, U. Köster, *et al.*, Further evidence for shape coexistence in ^{79}Zn^{m} near doubly magic ^{78}Ni, Phys. Rev. Lett. **131**, 222503 (2023).

[26] L. Nies, D. Atanasov, M. Athanasakis-Kaklamanakis, M. Au, C. Bernerd, K. Blaum, K. Chrysalidis, P. Fischer, R. Heinke, C. Klink, D. Lange, D. Lunney, V. Manea, B. A. Marsh, M. Müller, M. Mougeot, S. Naimi, C. Schweiger, L. Schweikhard, and F. Wienholtz, Refining the nuclear mass surface with the mass of ^{103}Sn, Phys. Rev. C **111**, 014315 (2025).

[27] D. Lange, D. Atanasov, M. Au, A. Belley, M. Benhatchi, K. Blaum, R. B. Cakirli, P. F. Giesel, A. Herlert, J. D. Holt, B. S. Hu, A. Jaries, C. Klink, Y. A. Litvinov, D. Lunney, V. Manea, F. Mehlhorn, T. Miyagi, M. Mougeot, S. Naimi, *et al.*, Constraining the trend of the $N = 50$ shell gap towards ^{100}Sn with the masses of $^{96-98}$Cd, arXiv:2604.18287.

[28] A. T. Bondy and G. W. F. Drake, Charge-state distributions after beta decay of ^{6}He to form ^{6}Li^{+}, Atoms **11**, 41 (2023).

[29] A. Kramida, Y. Ralchenko, J. Reader, and NIST ASD Team, NIST atomic spectra database (ver. 5.11), National Institute of Standards and Technology, Gaithersburg, MD (2023), https://physics.nist.gov/asd.

[30] P. J. Linstrom and W. G. Mallard, NIST chemistry WebBook, National Institute of Standards and Technology Standard Reference Database Number 69 (2023), https://webbook.nist.gov.

[31] National Nuclear Data Center, NuDat 3: Nuclear structure and decay data (2025).
[32] N. Nica, Nuclear data sheets for A = 97, Nucl. Data Sheets **111**, 525 (2010).
[33] W. Bambynek, B. Crasemann, R. W. Fink, H.-U. Freund, H. Mark, C. D. Swift, R. E. Price, and P. V. Rao, X-ray fluorescence yields, Auger, and Coster-Kronig transition probabilities, Rev. Mod. Phys. **44**, 716 (1972).